z_{0s} is the spread of the ground-state wavefunction for one ion in the stretch mode and ϕ_L is the phase of the driving field. Evaluation of the integrals in equation (8) yields:

$$\alpha_{\downarrow\uparrow}(\tau) = i\Omega_D/\delta[\exp(-i\delta\tau) - 1]\exp(i\phi_L)$$
$$\Phi_{\downarrow\uparrow}(\tau) = (\Omega_D/\delta)^2[\sin(\delta\tau) - \delta\tau] \quad (12)$$

For the π-phase gate the maximum excursion in phase space is $|\alpha_{\uparrow\downarrow\max}| = 1$. The normalized fluorescence is equal to:

$$S_{norm}(\tau) = P_{\downarrow\downarrow}(\tau) + 1/2[P_{\downarrow\uparrow}(\tau) + P_{\uparrow\downarrow}(\tau)] = 1/2[1 + \exp(-|\alpha_{\uparrow\downarrow}(\tau)|^2/2)\cos(\Phi_{\uparrow\downarrow}(\tau))] \quad (13)$$

For the fit in Fig. 3 we allowed for an additional exponential decay:

$$S_{fit}(\tau) = 1/2[1 + \exp(-\tau/\tau_0)\exp(-|\alpha_{\uparrow\downarrow}(\tau)|^2/2)\cos(\Phi_{\uparrow\downarrow}(\tau))] \quad (14)$$

where τ_0 is a phenomenological decay constant mimicking decoherence effects.

Gate speed considerations

The gate speed in our experiments was limited by the intensity of the displacement beams. The observed ratio of gate time $2\pi/\delta$ to stretch oscillation period $2\pi\omega_S$ was 238. The largest contribution to gate infidelity from off-resonant excitations is that due to excitation of the centre-of-mass (COM) mode (as opposed to excitation of the internal-state carrier transition in the Cirac–Zoller and Sørensen–Mølmer gates). The ratio of excitation amplitude of the stretch mode to that of the COM mode scales as δ_{COM}/δ where $\delta_{COM} \propto \omega_S$ is the detuning from the COM mode. Therefore if the required fidelity restricts the COM mode excitation to be below a certain size, then the gate rate ($\propto \delta$) will scale linearly with ω_S. For our experimental parameters, we estimate the contribution to infidelity from off-resonant excitation of the COM mode to be below 10^{-4}. In a more refined scenario, we could intentionally excite both the COM and the stretch mode. For suitable parameters the COM and stretch-mode amplitudes can return to their initial values even if the gate rate exceeds the trap frequency.

Received 18 December 2002; accepted 7 February 2003; doi:10.1038/nature01492.

1. Cirac, J. I. & Zoller, P. Quantum computations with cold trapped ions. *Phys. Rev. Lett.* **74,** 4091–4094 (1995).
2. Sørensen, A. & Mølmer, K. Quantum computation with ions in thermal motion. *Phys. Rev. Lett.* **82,** 1971–1974 (1999).
3. Sackett, C. A. *et al.* Experimental entanglement of four particles. *Nature* **404,** 256–259 (2000).
4. Wineland, D. J. *et al.* Experimental issues in coherent quantum-state manipulation of trapped atomic ions. *J. Res. Natl Inst. Stand. Technol.* **103,** 259–328 (1998).
5. Kielpinski, D., Monroe, C. & Wineland, D. J. Architecture for a large-scale ion-trap quantum computer. *Nature* **417,** 709–711 (2002).
6. Monroe, C., Meekhof, D. M., King, B. E., Itano, W. M. & Wineland, D. J. Demonstration of a fundamental quantum logic gate. *Phys. Rev. Lett.* **75,** 4714–4717 (1995).
7. Roos, Ch. *et al.* Quantum state engineering on an optical transition and decoherence in a Paul trap. *Phys. Rev. Lett.* **83,** 4713–4716 (1999).
8. Sørensen, A. & Mølmer, K. Entanglement and quantum computation with ions in thermal motion. *Phys. Rev. A* **62,** 02231 (2000).
9. DeVoe, R. G. Elliptical ion traps and trap arrays for quantum computation. *Phys. Rev. A* **58,** 910–914 (1998).
10. Cirac, J. I. & Zoller, P. A scalable quantum computer with ions in an array of microtraps. *Nature* **404,** 579–581 (2000).
11. Rowe, M. A. *et al.* Transport of quantum states and separation of ions in a dual rf ion trap. *Quant. Inf. Comput.* **4,** 257–271 (2002).
12. Carruthers, P. & Nieto, M. M. Coherent states and the forced quantum oscillator. *Am. J. Phys.* **7,** 537–544 (1965).
13. Walls, D. F. & Milburn, G. J. *Quantum Optics* (Springer, Berlin, 1994).
14. Monroe, C., Meekhof, D. M., King, B. E. & Wineland, D. J. A "Schrödinger Cat" superposition state of an atom. *Science* **272,** 1131–1136 (1996).
15. Myatt, C. J. *et al.* Decoherence of quantum superpositions through coupling to engineered reservoirs. *Nature* **403,** 269–273 (2000).
16. Milburn, G. J., Schneider, S. & James, D. F. Ion trap quantum computing with warm ions. *Fortschr. Physik* **48,** 801–810 (2000).
17. Wang, X., Sørensen, A. & Mølmer, K. Multibit gates for quantum computing. *Phys. Rev. Lett.* **86,** 3907–3910 (2001).
18. Wineland, D. J. *et al.* Quantum information processing with trapped ions. Preprint quant-ph/0212079 available at ⟨http://arXiv.org⟩ (2002).
19. King, B. E. *et al.* Cooling the collective motion of trapped ions to initialize a quantum register. *Phys. Rev. Lett.* **81,** 1525–1528 (1998).
20. Rowe, M. A. *et al.* Experimental violation of a Bell's inequality with efficient detection. *Nature* **409,** 791–794 (2001).
21. Steane, A. *et al.* Speed of ion trap quantum information processors. *Phys. Rev. A* **62,** 042305 (2000).
22. Steane, A. Overhead and noise threshold of fault-tolerant quantum error correction. Preprint quant-ph/0207119 available at ⟨http://arXiv.org⟩ (2002).

Acknowledgements We thank J. Chiaverini, T. Schätz and A. Steane for comments on the manuscript. This work was supported by the US National Security Agency (NSA), the Advanced Research and Development Activity (ARDA). This is a publication of a US government agency.

Competing interests statement The authors declare that they have no competing financial interests.

Correspondence and requests for materials should be addressed to D.J.W. (e-mail: david.wineland@boulder.nist.gov).

An electronic Mach–Zehnder interferometer

Yang Ji, Yunchul Chung, D. Sprinzak, M. Heiblum, D. Mahalu & Hadas Shtrikman

Braun Center for Submicron Research, Department of Condensed Matter Physics, Weizmann Institute of Science, Rehovot 76100, Israel

Double-slit electron interferometers fabricated in high mobility two-dimensional electron gases are powerful tools for studying coherent wave-like phenomena in mesoscopic systems[1–6]. However, they suffer from low visibility of the interference patterns due to the many channels present in each slit, and from poor sensitivity to small currents due to their open geometry[3–5,7]. Moreover, these interferometers do not function in high magnetic fields—such as those required to enter the quantum Hall effect regime[8]—as the field destroys the symmetry between left and right slits. Here we report the fabrication and operation of a single-channel, two-path electron interferometer that functions in a high magnetic field. This device is the first electronic analogue of the optical Mach–Zehnder interferometer[9], and opens the way to measuring interference of quasiparticles with fractional charges. On the basis of measurements of single edge state and closed geometry transport in the quantum Hall effect regime, we find that the interferometer is highly sensitive and exhibits very high visibility (62%). However, the interference pattern decays precipitously with increasing electron temperature or energy. Although the origin of this dephasing is unclear, we show, via shot-noise measurements, that it is not a decoherence process that results from inelastic scattering events.

Direct phase measurements of electrons, customarily done in double-slit interferometers[1–4], are difficult to perform under strong magnetic fields. Electrons are diverted by the Lorentz force, perform chiral skipping orbits, and prefer one slit to the other—thus breaking the symmetry of the interferometer. At the extreme quantum limit (that is, in the quantum Hall effect, QHE, regime), the skipping orbits quantize to quasi-one-dimensional-like states, named chiral edge states. We have exploited the chiral motion of the electrons, and constructed an electronic analogue of the ubiquitous optical Mach–Zehnder interferometer[9] (Fig. 1a). A beam splitter BS1 splits an incoming monochromatic light beam from source S into two beams, which, after reflection by mirrors M1 and M2, recombine and interfere at BS2 to result in two outgoing beams (collected by detectors D1 and D2). When the phase along one of the paths varies, signals in both D1 and D2 oscillate out of phase, and as no photons are being lost, the sum of both signals stays always equal to the input, S. In the electronic counterpart (Fig. 1b), quantum point contacts (QPCs) function as beam splitters, and ohmic contacts serve as detectors. A QPC is formed in the two-dimensional electron gas (2DEG) by depositing a split metallic gate on the surface of the semiconductor and biasing it negatively with respect to the 2DEG. The induced potential in the 2DEG creates a barrier under the gate bringing the two oppositely propagating edge currents to the small opening in the barrier, thus allowing backscattering. As shown schematically in Fig. 1b, QPC1 splits the incoming edge current from S to two paths, a transmitted outer path and a reflected inner path; both later recombine and interfere in QPC2, resulting in two edge currents (collected by D1 and D2).

The actual device (Fig. 1c) was fabricated in a high-mobility 2DEG embedded in a GaAs–AlGaAs heterojunction. A ring-shaped mesa, 3 μm in width, was defined by plasma etching with ohmic contacts (for S, D1 and D2) connected to the inner and outer edges of the ring. The inner contact, D2, and the two QPCs are connected to outside sources via metallic films that hover above the surface of

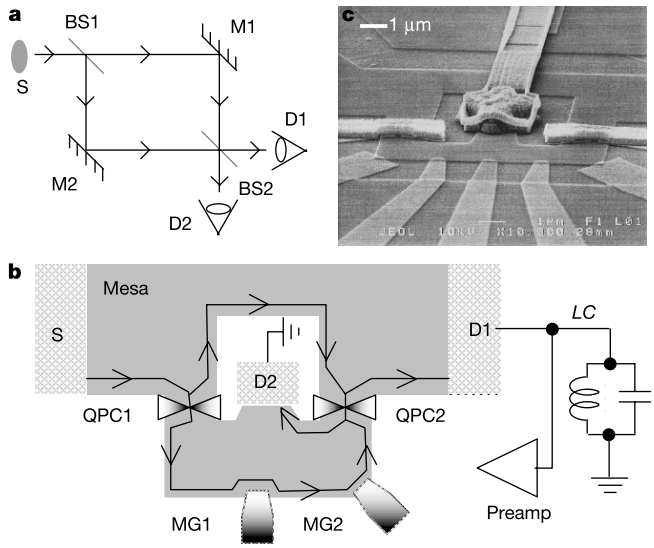

Figure 1 The configuration and operation of an optical Mach–Zehnder interferometer, and its realization with electrons. **a**, An optical Mach–Zehnder interferometer. D1 and D2 are detectors, BS1 and BS2 are beam splitters, and M1 and M2 are mirrors. With 0 (π) phase difference between the two paths, D1 measures maximum (zero) signal and D2 zero (maximum) signal. The sum of the signals in both detectors is constant and equal to the input signal. **b**, The electronic Mach–Zehnder interferometer and the measurement system. Edge states are formed in a high, perpendicular, magnetic field. The incoming edge state from S is split by QPC1 (quantum point contact 1) to two paths; one moves along the inner edge, and the other along the outer edge, of the device. The two paths meet again at QPC2, interfere, and result in two complementary currents in D1 and in D2. By changing the contours of the outer edge state and thus the enclosed area between the two paths, the modulation gates (MGs) tune the phase difference between the two paths via the Aharonov–Bohm effect. A high signal-to-noise-ratio measurement of the current in D1 is performed at 1.4 MHz with a cold *LC* resonant circuit as a band-pass filter followed by a cold, low-noise, preamplifier. **c**, Scanning electron micrograph of the device. A centrally located small ohmic contact ($3 \times 3\,\mu m^2$), serving as D2, is connected to the outside circuit by a long, metallic, air bridge. Two smaller metallic air bridges bring the voltage to the inner gates of QPC1 and QPC2—both serve as beam splitters for edge states. The five metallic gates (at the lower part of the figure) are MGs.

the mesa, called 'air bridges'. A phase difference φ between the two paths is introduced via the Aharonov–Bohm (AB) effect[10,11], $\varphi = 2\pi BA/\phi_0$, with B the magnetic field, A the area enclosed by the two paths ($\sim 45\,\mu m^2$), and $\phi_0 = 4.14 \times 10^{-15}\,T\,m^2$ the flux quantum. A few modulation gates, MG, are added above the outer path in order to tune the phase φ by changing the area A.

We briefly review the operation of the interferometer. At filling factor 1 in the QHE regime, a single chiral edge state carries the current. The interfering current, in turn, is proportional to the transmission probability from source to drain, T_{SD}. Neglecting dephasing processes and having the transmission (reflection) amplitude t_i (r_i) of the ith QPC fulfilling $|r_i|^2 + |t_i|^2 = 1$, then[7] $I_{D1} \propto T_{SD1} = |t_1 t_2 + r_1 r_2 e^{i\varphi}|^2 = |t_1 t_2|^2 + |r_1 r_2|^2 + 2|t_1 t_2 r_1 r_2|\cos\varphi$ and $I_{D2} \propto T_{SD2} = |t_1 r_2 + r_1 t_2 e^{i\varphi}|^2 = |t_1 r_2|^2 + |r_1 t_2|^2 - 2|t_1 t_2 r_1 r_2|\cos\varphi$, where I_{D1} and I_{D2} are the currents in detectors D1 and D2, respectively. Note that ideally the two currents oscillate out of phase as function of φ while $T_{SD1} + T_{SD2} = 1$. The visibility of the oscillation is defined as: $\nu = (I_{max} - I_{min})/(I_{max} + I_{min})$, where I_{max} and I_{min} are the maximum and minimum currents in one of the detectors. For example, when QPC2 is tuned so that $T_2 = 0.5$, the visibility is $\nu = 2\sqrt{T_1(1 - T_1)}$, where $|t_i|^2 = T_i$.

Measurements were done at filling factor 1 (magnetic field $\sim$5.5 T) and also at filling factor 2 with similar results. With a refrigerator temperature of $\sim$6 mK, the electron temperature was determined by measuring the equilibrium noise[12] to be $\sim$20 mK. High-sensitivity measurements of the interference pattern were conducted at $\sim$1.4 MHz with a spectrum analyser. Current at D1 (or D2) was filtered and amplified *in situ* by an *LC* (inductance + capacitance) circuit and a low-noise, purpose-built pre-amplifier, both placed near the sample and cooled to 1.5 K. A standard lock-in technique, with a low-frequency signal (7 Hz, 10 μV r.m.s.), gave similar results, but the measurement lasted much longer and was affected by the instability of the sample. At 5.5 T, each flux quantum occupies an area of some $10^{-15}\,m^2$ (some 60,000 flux quanta thread the area A), so a minute fluctuation in the superconducting magnet's current or in the area would smear the interference signal. Two measurement methods were used. The first relied on the unavoidable decay of the short-circuited current that circulates in the superconducting magnet, which is in the so-called

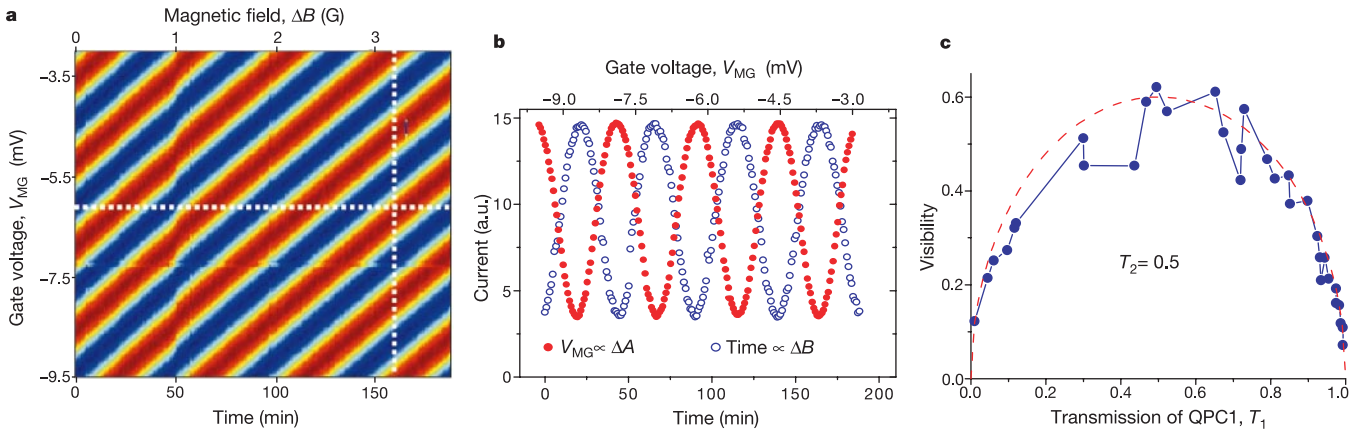

Figure 2 Interference pattern of electrons in a Mach–Zehnder interferometer and the dependence on transmission. **a**, Two-dimensional colour plot of the current collected by D1 as function of magnetic field and gate voltage at an electron temperature of $\sim$20 mK. The magnet was set in its persistent current mode ($B \approx 5.5$ T at filling factor 1 in the bulk) with a decay rate of some 0.12 mT h^{-1}, hence time appears on the abscissa. The two QPCs were both set to transmission $T_1 = T_2 = 0.5$. Red (blue) stands for high (low) current. **b**, The current (a.u., arbitrary units) collected by D1 plotted as function of the voltage on a modulation gate, V_{MG} (red plot), and as function of the magnetic field, B (blue plot)—along the cuts shown in **a**. The visibility of the interference is 0.62. **c**, The visibility of the interference pattern (data points) as a function of the transmission probability T_1 of QPC1 when QPC2 is set to $T_2 = 0.5$. Red dashed line is a fit to the experimental data with visibility $2\eta\sqrt{T_1(1 - T_1)}$. The normalization coefficient $\eta = 0.6$ accounts for possible decoherence and/or phase averaging.

persistent current mode. In this mode, the magnetic field decays smoothly at a rate of $\sim 0.12\,\mathrm{mT\,h^{-1}}$ (~ 1 flux quantum every 50 min). The second was via scanning the voltage on a modulation gate at a rate much faster than the decay rate of the magnetic field, thus changing the area A, the enclosed flux, and consequently the AB phase.

We first test the ideality of the ohmic contacts and the validity of the edge-states picture. For both QPCs open, a nearly ideal Hall plateau was observed in I_{D1} while no current was measured in D2 ($I_{D2} = 0$). This confirms that current was confined to the outer edge with no backscattering across the 3-μm-wide mesa. We then pinched off QPC1 or QPC2, and found again a Hall plateau in I_{D2} with zero current in D1 ($I_{D1} = 0$). This proved that the small ohmic contact of D2 was ideal and fully absorbed the current. Setting then both QPCs to $T_1 = T_2 \approx 1/2$ and varying the magnetic field B (actually the time) or the area A (the voltage on a MG) led to a pronounced interference signal in D1 (or in D2) with visibility as high as 0.62 (Fig. 2). As the field decays linearly with time, and the area (or electron density) varies in proportion to the gate voltage, changing these parameters leads to the diagonal, straight, lines of colour (of constant phase) seen in Fig. 2a. Figure 2b shows similar data taken along two cuts (the dotted lines shown in Fig. 2a)—one for constant B and one for constant A. The cleanliness of the interference pattern and the high visibility prove the nearly ideal nature of the interferometer.

In order to verify further the two-path nature of the interference, the visibility was measured as function of T_1 for a constant $T_2 = 0.5$ (Fig. 2c). It agrees well with the expected expression, $\nu = 2\eta\sqrt{T_1}(1 - T_1)$, with $\eta \approx 0.6$ a normalization factor that accounts for dephasing (either due to phase averaging in the energy window of the electrons, or due to inelastic scattering processes). Moreover, the period of the oscillations, in time and in MG voltage, agrees well with one flux quantum being added (or subtracted) in the ring's area. The time period is ~50 min, which is the time needed for one flux quantum decay in the superconducting magnet, while the voltage period agrees approximately with that needed to deplete one electron (hence, one flux quantum for filling factor 1) under the MG gate.

Although the visibility is very high, it is still smaller than unity ($\nu \approx 0.6$). An obvious reason for this is the finite energy spread of the electrons at the edge (due to their finite temperature), and the unavoidable dependence of the AB area on the energy (hence, the AB phase)—leading to phase averaging (thermal smearing). Indeed, the visibility was found to drop precipitously with increasing temperature or applied voltage at S, as seen in Fig. 3. In this example, a mere increase of the temperature to 100 mK (some ~9 μeV) reduced the visibility from $\nu \approx 0.53$ to $\nu \approx 0.01$ (plotted in red in Fig. 3a). If indeed phase averaging is the cause of the dephasing, it could, in principle, be eliminated with monoenergetic electrons. A minute a.c. signal (~0.5 μV) at 1.4 MHz was added to a variable d.c. voltage V_{dc} and the synchronous a.c. part of the interfering signal was measured at 20 mK. This signal leads to a differential visibility ν_d, resulting only from the electrons in an energy window ~0.5 μeV around an energy eV_{dc}. Surprisingly, as seen in Fig. 3a (plotted in blue), the energy-dependent differential visibility at $T = 20$ mK is similar to the temperature-dependent visibility, with a relation between the scales $eV_{dc} \approx 4k_BT$. The visibility (in colour scale) is plotted as function of both T and V_{dc} in Fig. 3b. The clear symmetry across the diagonal suggests that the dephasing processes due to temperature and voltage are similar. Unfortunately, this contradicts our previous assertion of phase averaging taking place in a wide window of energy, and points at decoherence, induced by inelastic scattering events, as the main source of dephasing. In other words, for an increased temperature or for high-energy monoenergetic electrons, empty states are being created, allowing energy loss via scattering.

In order to test this hypothesis, current shot noise was measured. Its spectral density is defined as the averaged square of the current

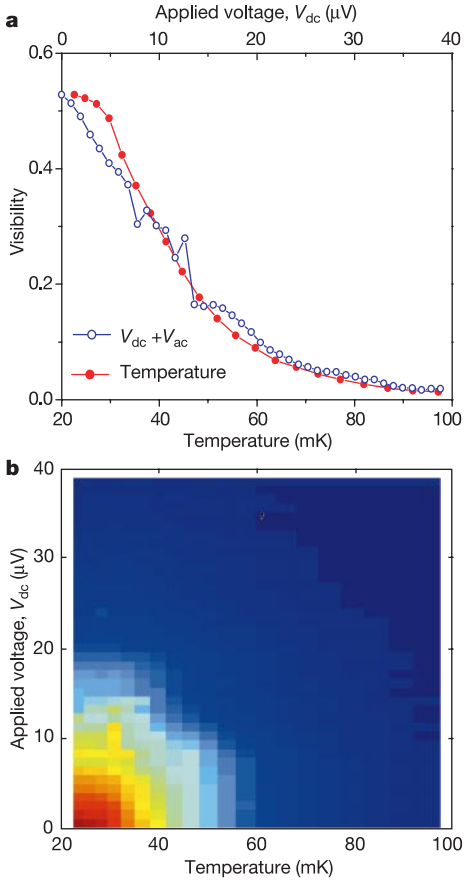

Figure 3 The dependence of the visibility of the interference pattern on temperature and applied voltage. **a**, Visibility as function of temperature at small excitation voltage for $V_{dc} = 0$ (red plot), and as function of V_{dc} with a small a.c. voltage V_{ac} superimposed on it at electron temperature 20 mK (blue plot). Both QPCs were set to $T_1 = T_2 = 0.5$. **b**, A two-dimensional colour plot of the visibility as function of temperature and applied d.c. voltage. Red (blue) stands for high (low) visibility.

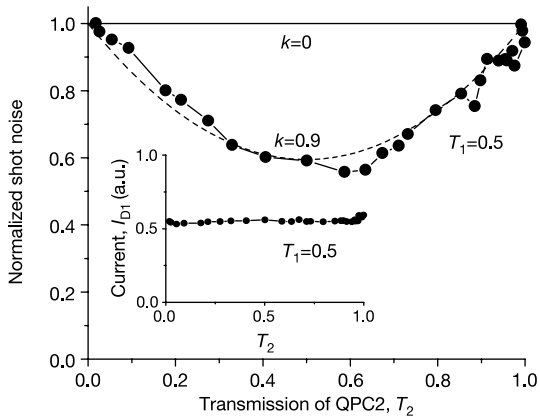

Figure 4 Shot-noise measurement (at filling factor 2) as function of T_2 when the transmission of QPC1 was set to $T_1 = 0.5$. A 30-μV d.c. voltage (under which the AB interference pattern was quenched) was used to measure shot noise. The shot noise of the current collected by D1 is shown by the black dots (normalized to a maximum), while the two solid lines are the expected noise for $k = 0$ and $k = 0.9$, respectively, according to the simple model described in the text. The agreement with the simple model indicates that the electrons are coherent even at the d.c. voltage where the interference pattern fades away. Inset, the current at D1 as function of T_2 at $V_{dc} = 30$ μV. As expected from the lack of the interference pattern, the current is independent of T_2 (see text).

fluctuations per unit of frequency, $S = \langle(i^2)\rangle/\Delta f$; for stochastic partitioning at zero temperature, $S \propto eV_{dc}T_{SD}(1 - T_{SD})$ (ref. 13). Introducing a phenomenological parameter k that accounts for decoherence in the interferometer with $T_1 = 1/2$ and $T_{SD} = 0.5 + k\sqrt{T_2(1 - T_2)}\cos\varphi$, we find that for complete phase averaging or for a complete decoherence $T_{SD} = 0.5$, namely, a constant. On the other hand, shot noise in D1 is $S_{D1} \propto T_{SD1}(1 - T_{SD1}) = 1/4 - k^2T_2(1 - T_2)\cos^2\varphi$, with $S_{D1} =$ const. for $k = 0$, but $S_{D1} = 1/4 - k^2T_2(1 - T_2)/2$ for complete phase averaging (resulting from an integration of $\cos^2\varphi$ in the range $\varphi = 0\ldots\ldots2\pi$). Hence, noise is expected to exhibit a parabolic dependence on T_2 in a coherent system. Shot noise was measured[12,13] with a relatively large V_{dc} applied at S so that interference signal was quenched (negligible visibility). The dependence of S on T_2, shown in Fig. 4, followed the above expression with $k \approx 0.9$, proving that phase averaging is indeed dominant while decoherence is negligibly small.

A single-particle model (that is, a non-interacting model) would lead to the following dependences of the visibility on energy: for $V = 0$ and finite T, $\nu \propto \beta T/\sinh(\beta T)$, with β a constant; for finite V but $T = 0$, $\nu \propto \sin[(e/2\pi)V]/[(e/2\pi)V]$, while the differential visibility at $T = 0$ is expected to be voltage independent. Because the experimental results contradict these predictions, we propose (with no proof yet) two possible reasons for the dephasing. One might be low-frequency noise (of, say, the $1/f$ type due to moving impurities), which might be induced by a higher current, leading to fluctuation in the area and consequently, phase smearing. The other could be related to the self-consistent potential contour at the edge. As it depends on the local density of the electrons in the edge state[14], fluctuation in the density due to partitioning are expected to lead to fluctuation in the AB area enclosed by the two paths and hence to phase randomization. For example, for $B \approx 5.5$ T, a shift of the edge of only 1–2 Å suffices to add one flux quantum into the enclosed area.

We believe that this electron interferometer might prove useful in future work on the interference of electrons. One possible area of research is the coherence and phase of fractionally charged quasiparticles in the fractional QHE regime[15]. □

Received 1 October 2002; accepted 12 February 2003; doi:10.1038/nature01503.

1. Yacoby, A., Heiblum, M., Umansky, V., Shtrikman, H. & Mahalu, D. Unexpected periodicity in an electronic double slit interference experiment. *Phys. Rev. Lett.* **73,** 3149–3152 (1994).
2. Yacoby, A., Heiblum, M., Mahalu, D. & Shtrikman, H. Coherency and phase sensitive measurements in a quantum dot. *Phys. Rev. Lett.* **74,** 4047–4050 (1994).
3. Schuster, R. *et al.* Phase measurement in a quantum dot via a double-slit interference measurement. *Nature* **385,** 417–420 (1997).
4. Ji, Y., Heiblum, M., Sprinzak, D., Mahalu, D. & Shtrikman, H. Phase evolution in a Kondo-correlated system. *Science* **290,** 779–783 (2000).
5. Buks, E., Schuster, R., Heiblum, M., Mahalu, D. & Shtrikman, H. Dephasing in electron interference by a 'which-path' detector. *Nature* **391,** 871–820 (1998).
6. van der Viel, W. G. *et al.* The Kondo effect at unitary limit. *Science* **289,** 2105–2108 (2000).
7. Buttiker, M. Four terminal phase coherent conductance. *Phys. Rev. Lett.* **57,** 1761–1764 (1986).
8. Prange, R. E. & Girvin, S. M. (eds) *The Quantum Hall Effect* (Springer, New York, 1987).
9. Born, M. & Wolf, E. *Principles of Optics* 348–352, 7th edn (Cambridge Univ. Press, Cambridge, UK, 1999).
10. Aharonov, Y. & Bohm, D. Significance of electromagnetic potentials in the quantum theory. *Phys. Rev.* **115,** 485–491 (1959).
11. Aronov, A. G. & Sharvin, Yu. V. Magnetic flux effects in disordered conductors. *Rev. Mod. Phys.* **59,** 755–779 (1987).
12. de-Picciotto, R. *et al.* Direct observation of a fractional charge. *Nature* **389,** 162–165 (1997).
13. Reznikov, M. *et al.* Quantum shot noise. *Superlattice Microstruct.* **23,** 901–915 (1998).
14. Chklovskii, D. B., Shklovskii, B. I. & Glazman, L. I. Electrostatics of edge channels. *Phys. Rev. B* **46,** 4026–4034 (1992).
15. Kane, C. L. Telegraph noise and fractional statistics in the quantum Hall effect. Preprint cond-mat/0210621 at ⟨http://xxx.lanl.gov⟩ (2002).

Acknowledgements We thank Y. Levinson for clarifying the issue of phase averaging, and C. Kane for comments on the manuscript. The work was partly supported by the MINERVA Foundation, the Israeli Academy of Science, the German Israeli Project Cooperation (DIP), the German Israeli Foundation (GIF), and the EU QUACS network.

Competing interests statement The authors declare that they have no competing financial interests.

Correspondence and requests for materials should be addressed to M.H. (e-mail: heiblum@wisemail.weizmann.ac.il).

African vegetation controlled by tropical sea surface temperatures in the mid-Pleistocene period

Enno Schefuß*, Stefan Schouten, J. H. Fred Jansen & Jaap S. Sinninghe Damsté

Royal Netherlands Institute for Sea Research (NIOZ), PO Box 59, 1790 AB Den Burg, The Netherlands

The dominant forcing factors for past large-scale changes in vegetation are widely debated. Changes in the distribution of C_4 plants—adapted to warm, dry conditions and low atmospheric CO_2 concentrations[1]—have been attributed to marked changes in environmental conditions, but the relative impacts of changes in aridity, temperature[2,3] and CO_2 concentration[4,5] are not well understood. Here, we present a record of African C_4 plant abundance between 1.2 and 0.45 million years ago, derived from compound-specific carbon isotope analyses of wind-transported terrigenous plant waxes. We find that large-scale changes in African vegetation are linked closely to sea surface temperatures in the tropical Atlantic Ocean. We conclude that, in the mid-Pleistocene, changes in atmospheric moisture content—driven by tropical sea surface temperature changes and the strength of the African monsoon—controlled aridity on the African continent, and hence large-scale vegetation changes.

Two main carbon fixation pathways of higher plant photosynthesis, the Calvin–Benson (C_3) and the Hatch–Slack (C_4) cycles, occur in natural ecosystems[6]. Nearly all trees, cold-season grasses and sedges use the C_3 pathway, whereas C_4 photosynthesis is found in warm-season grasses and sedges[7]. Thus, C_4 plants are found predominantly in tropical savannahs, temperate grasslands and semideserts[7]. Most African grasslands are dominated currently by C_4 plant vegetation[1]. C_4 plants use a CO_2-concentrating mechanism, thereby outcompeting C_3 plants at low atmospheric p_{CO_2} (ref. 8) and causing them to be isotopically enriched in ^{13}C (ref. 4). At high p_{CO_2}, however, C_3 plants will outcompete C_4 plants owing to the higher energy need of C_4 plants during photosynthesis[8]. The crossover between C_3 and C_4 plants depends also on the daytime growing-season temperature, with higher temperatures favouring C_4 plants[7,8]. Other factors, however, may also affect the occurrence of C_3 and C_4 plants. Where precipitation and nutrient availability permit trees to grow, C_3 trees will outcompete C_4 grasses, such as in the tropical forests[1]. The significance of the climatic factors determining the large-scale C_4 plant abundance is still not well understood, but insights can be gained from the analysis of past vegetation changes.

Long-chain, odd-numbered C_{25} to C_{35} *n*-alkanes are major lipid constituents of the epicuticular wax layer of terrestrial plants[9]. These plant waxes are easily removed from the leaf surface by rain or wind, especially by sandblasting during dust storms. They are, therefore, common organic components of eolian dust[10]. In surface sediments of the eastern South Atlantic, the plant wax *n*-alkanes exhibit a moderate to high odd versus even carbon-number predominance (carbon preference index (CPI) of 2.3–6.4), and thus predominantly represent leaf waxes of terrestrial higher plants[9]. Their plume-like distribution in surface sediments (Fig. 1a) indicates that they are primarily transported by southeasterly winds from the dry areas in southern Africa, the Kalahari savannah and Namib Desert. The discharge of the Congo River is apparently of minor importance for the supply of *n*-alkane leaf waxes. During the austral winter (June to August) the strong Southern Hemisphere trade winds transport

* Present address: Research Center Ocean Margins, University of Bremen, PO Box 330440, 28334 Bremen, Germany.